Enhanced stability of single-layer w-Gallenene through hydrogenation

THE JOURNAL OF PHYSICAL CHEMISTRY C

C: Physical Processes in Nanomaterials and Nanostructures

Enhanced Stability In Single-Layer *w*-Gallenene Through Hydrogenation

Sabuhi V. Badalov, Mehmet Yagmurcukardes, Francois M. Peeters, and Hasan Sahin

J. Phys. Chem. C, **Just Accepted Manuscript** • DOI: 10.1021/acs.jpcc.8b07353 • Publication Date (Web): 12 Nov 2018

ACS Publications

is published by the American Chemical Society. 1155 Sixteenth Street N.W., Washington, DC 20036

Enhanced Stability In Single-Layer *w*-Gallenene Through Hydrogenation

S. V. Badalov,[1,*] M. Yagmurcukardes,[2,†] F. M. Peeters,[2] and H. Sahin[1,3]

[1]*Department of Photonics, Izmir Institute of Technology, 35430, Izmir, Turkey*

[2]*Department of Physics, University of Antwerp, Groenenborgerlaan 171, B-2020 Antwerp, Belgium*

[3]*ICTP-ECAR Eurasian Center for Advanced Research, Izmir Institute of Technology, 35430, Izmir, Turkey*

(Dated: November 9, 2018)

Abstract

Using density functional theory-based first-principles calculations, the effect of surface hydrogenation on the structural, dynamical, electronic, and mechanical properties of monolayer washboard-gallenene (*w*-gallenene) is investigated. It is found that the dynamically stabilized strained-monolayer of *w*-gallenene has a metallic non-magnetic ground state. Both one-sided and two-sided hydrogenation of *w*-gallenene suppresses its dynamical instability even when unstrained. Unlike one-sided hydrogenated monolayer *w*-gallenene (os-*w*-gallenene), two-sided hydrogenated monolayer *w*-gallenene (ts-*w*-gallenene) possesses the same crystal structure as *w*-gallenene. Electronic band structure calculations reveal that monolayers of hydrogenated derivatives of *w*-gallenene exhibit also metallic non-magnetic ground state. Moreover, the linear-elastic constants, in-plane stiffness and Poisson ratio, are enhanced by hydrogenation which is opposite to the behavior of other hydrogenated monolayer crystals. Furthermore, monolayer *w*-gallenene and ts-*w*-gallenene remain dynamically stable up to relatively higher biaxial strains when compared to borophene. With its enhanced dynamical stability, robust metallic character, and enhanced linear-elastic properties, hydrogenated monolayer *w*-gallenene is a potential candidate for nanodevice applications as a 2D flexible metal.

PACS numbers:

I. INTRODUCTION

Since the successful isolation of graphene[1,2] from its bulk counterpart, graphite, two-dimensional (2D) materials have received immense interest in material science and device technology owing to their unconventional properties.[3–6] It has stimulated researchers to synthesize other monolayer mono-atomic crystals such as silicene,[7–9] germanene,[10–13] stanene,[14,15] phosphorene,[16] and borophene[17] which exhibit a wide range of electronic, thermal, mechanical, and chemical properties making them promising candidates for many different applications.

Gallium is an enchanting metallic element because it favors covalency over metallicity in its bulk form.[18] Therefore, gallium possesses one of the most diverse phase diagrams of the metallic elements, and it is a non-toxic liquid metal at room temperature.[19,20] It displays various types of phases such as a boron-like molecular and close-packed metallic phase under non-standard pressure and temperature.[19,21,22] Furthermore, the extreme covalent character of the Ga_2 pairs results in a dimer-like behavior. Hence, among the mono-atomic materials, α-Ga is the only one which exhibits both metallic and molecular character at zero-pressure.[19] On the other hand, gallium is known to form the basis of the following semiconductors: GaX (X = N, P, As), which are used primarily in electronic circuit and semiconductor devices.[20,23,24] Zhang *et al.* reported that epitaxially grown Ga films on the wide-band-gap semiconductor GaN(0001) demonstrate a novel platform for exploring atomic-scale 2D superconductors, which carry great potential for understanding interface superconductivity.[25] Zhou *et al.* showed that the strongest second-harmonic generation intensity is observed for GaSe among 2D crystals.[26] Moreover, 2D GaS and GaO layers with exciting functional properties were also successfully synthesized.[27] In our recent study, we reported that monolayers of Ga-monochalcogenides (GaS and GaSe) are ductile and flexible materials.[28]

Apart from its binary compounds, mono-atomic crystals of gallium in the 2D limit has not been studied in detail up to date. Xing *et al.* reported that the quantum Griffiths singularity is observed experimentally in atomically thin gallium films by showing a superconductor-metal transition with increasing magnetic field.[29] Very recently, Kochat *et al.* reported the successful synthesis of two dimensional atomically thin gallenene phases on various substrates.[30] They also showed that free-standing "gallenene" can be dynamically stabilized upon the application of biaxial strain.

Surface functionalization is an alternative approach to strain that can improve the stability of 2D materials and for tuning their structural,[31,32] electronic,[33,34] and magnetic[35] properties. Generally, hydrogenation is utilized experimentally for surface functionalization because it is a simple and versatile method.[36] Here, motivated by a recent study which revealed highly anisotropic, partially filled Dirac cones and non-linear dispersive bands in w-gallenene, we present a comprehensive investigation of the surface functionalization of w-gallenene via one- and two-sided hydrogenation. The effect of hydrogenation on the structural, phononic, electronic, and mechanical properties of w-gallenene are investigated in detail.

The paper is organized as follows: The computational methodology is given in Sec. II. The structural, vibrational, and electronic properties of pristine w-gallenene are discussed in Sec. III A. The adsorption of a single H atom and a H_2 molecule on w-gallenene are presented in Sec. III B 1. The properties of monolayers of os-w-gallenene and ts-w-gallenene are presented in Secs. III B 2 and III B 3, respectively. The mechanical properties of all monolayers of w-gallenene crystals as their linear-elastic constants: in-plane stiffness and Poisson ratio are discussed in Sec III C. We conclude in Sec. IV.

II. COMPUTATIONAL DETAILS

First-principles calculations were performed within the density functional theory (DFT) formalism by using the Vienna *ab-initio* Simulation Package (VASP).[38] In order to approximate the exchange and correlation energies, Perdew-Burke-Ernzerhof (PBE) form of the generalized gradient approximation (GGA) functional was used. Analysis of the charge transfers between individual atoms were determined by the Bader technique.[39]

The kinetic energy cut-off for plane-wave expansion was set to 500 eV and the energy was minimized until its variation in the following steps became less than 10^{-8} eV and Hellmann-Feynman forces on each unit cell was taken to be less than 10^{-7} eV/Å. $19 \times 19 \times 1$ Γ-centered k-point sampling was used for the primitive unit cell for band structure calculations performed within spin-orbit coupling (SOC). The metallicity of monolayers of Gallenene and its derivatives are also examined by performing electronic band structure calculations including local density approximation (LDA), Heyd-Scuseria-Ernzerhof (HSE) and META-GGA functionals (see Figure S1 in the Supporting Information (SI)). The Methfessel-Paxton

Table 1: The calculated parameters for monolayers of bare w-gallenene and its hydrogenated derivatives; the lattice constants, a and b the atomic distance between two Ga atoms, δ_1 and δ_2; the thickness of the monolayer structure, t; the charge donation from Ga to H, $\Delta\rho_{Ga-H}$; the magnetization μ; the cohesive energy per atom, $E_{Coh/atom}$, and Φ is the work function. The in-plane stiffness, C_a and C_b, and Poisson ratio, ν_a and ν_b.

	a (Å)	b (Å)	δ_1 (Å)	δ_2 (Å)	t (Å)	$\Delta\rho_{Ga-H}$ (e^-)	μ (μ_B)	$E_{Coh/atom}$ (eV)	Φ (eV)	C_a (N/m)	C_b (N/m)	ν_a –	ν_b –
bare	4.65	4.82	2.71	2.73	1.27	-	0	2.32	4.03	25	25	0.20	0.20
os	4.65	4.65	2.82	2.90	3.70	0.2	0	2.25	5.17	52	52	0.26	0.26
ts	4.62	4.55	2.72	2.66	4.44	0.3	0	2.25	5.22	48	47	0.25	0.25

scheme broadening for the density of states calculation was taken to be 0.2 eV. To avoid interaction between adjacent layers, a vacuum space of ∼15 Å was implemented. The phonon dispersions were calculated by using the PHON code[40], which uses the force constants calculated with the small-displacement method. The cohesive energy per atom E_{Coh} was

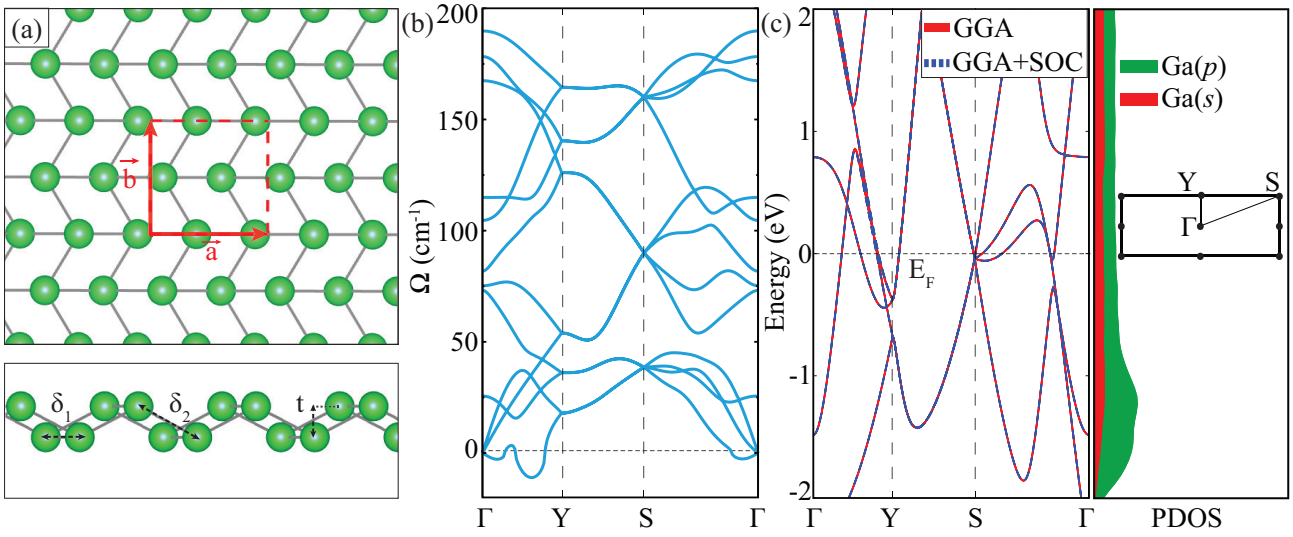

Figure 1: (Color online) (a) Top and side views of monolayer w-gallenene. Red dashed lines represent the rectangular unit cell; $\vec{a}$ and $\vec{b}$ are the lattice vectors. (b) The phonon band diagram of w-gallenene. (c) The electronic band diagram and orbital projected partial density of states of w-gallenene. Inset represents the high symmetry points in the first BZ of the orthorhombic reciprocal unit cell. The Fermi level is set to zero.

calculated using:

$$E_{Coh} = \frac{1}{n_{tot}} \left[\sum_{i=1} n_i E_i - E_{sl} \right], \quad (1)$$

where E_i represents the energies of a single isolated atom and the i index denotes the type of atom. E_{sl} represents the total ground state energy of the related monolayer structures, n_{tot} and n_i are the total number of atoms and the number of isolated i type atoms within the computational unit cell, respectively. The binding energy of an adsorbed atom and molecule was calculated as:

$$E_b = E_{sl} + E_{ad} - E_{sl+ad}, \quad (2)$$

where E_{sl} denotes the energy of the monolayer, E_{ad} is the energy of an isolated adatom or admolecule, E_{sl+ad} denotes the total energy when the adatom or admolecule is adsorbed on the monolayer. In addition, the thermal stability of the all monolayer Gallenene crystals were examined by performing *ab-initio* molecular dynamics (MD) calculations (see Figure S2 in the SI).

III. RESULTS

A. WASHBOARD STRUCTURE OF SINGLE-LAYER GALLENENE

In this section, the structural, electronic, and vibrational properties of w-gallenene, a single plane of bulk α-Ga exfoliated along the (010) direction, are investigated. This monolayer is the most suitable gallenene phase for hydrogenation and is similar to the anisotropic structure of w-borophene.[17] The optimized atomic structure of w-gallenene resembles a zigzag orthorhombic structure which is like a washboard structure. As shown in Figure 1(a), it forms a 2D double-decker structure, where the two Ga atoms are separated by t=1.27 Å along the out-of-plane direction which is defined as the buckling height. The primitive unit cell of the structure includes four Ga atoms. The lattice constants of the primitive unit cell are calculated to be a=4.65 Å and b=4.82 Å. The Ga-Ga bond lengths are found to be δ_1 =2.71 Å and δ_2=2.73 Å. It is revealed that the non-magnetic ground state of w-gallenene is formed with a cohesive energy of 2.32 eV/atom. In addition, as given in Table 1, the work function (WF) of monolayer w-gallenene is ∼4.03 eV which is less than that of graphene (∼ 4.6 eV).[41]

For a reliable analysis of the dynamical stability of the w-gallenene sheet, it is required to examine the phonon band structure in the whole BZ. The unit cell of w-gallenene consists of 4 atoms, which yields 12 phonon branches, 3 of which are acoustic (longitudinal acoustic (LA), transverse acoustic (TA) and out-of-plane flexural (ZA)) while the other 9 are optical phonon branches. The force constant matrix is calculated by displacing the atoms from their equilibrium positions in a $5 \times 5 \times 1$ supercell. It is found that w-gallenene is dynamically unstable since its phonon dispersion displays imaginary frequencies between the Γ and Y high symmetry points as shown in Figure 1(b). However, the instability of monolayer w-gallenene is suppressed by applying 2% of biaxial strain which can be realized by an appropriate substrate. Furthermore, due to atomic mass and bonding type of Ga atoms, the phonon modes of w-gallenene lie at much lower energies when compared to those of other 2D materials such as graphene ($\sim$1500 cm^{-1}), silicene ($\sim$580 cm^{-1}), and h-BN ($\sim$1600 cm^{-1}).[45–47]

The electronic properties of w-gallenene are investigated in terms of its electronic band structure and corresponding orbital projected partial density of states (PDOS) as shown in Figure 1(c). It is found that w-gallenene possesses metallic character. Unlike other 2D mono-atomic materials, the bands are highly dispersive with a large bandwidth and increased anisotropy in the low-energy bands. Therefore, w-gallenene exhibits lighter charge carriers and higher mobilities. In addition, it is seen in Figure 1(c) that the SOC has a negligibly small effect on the electronic band structure. Moreover, PDOS shows that the conduction band (CB) and valence band (VB) states are mainly made up of the p-orbitals of the Ga atoms.

B. HYDROGENATION OF *w*-gallenene

In this section, enhanced dynamical stability of monolayer w-gallenene is found via one-sided and two-sided hydrogenations. Monolayer w-gallenene was successfully synthesized on SiO_2 substrate and can be dynamically stabilized upon application of biaxial strain[30] which can be realized by an appropriate substrate. A question naturally arises whether the dynamical instability of free-standing w-gallenene can be suppressed only by biaxial strain or is there any other possible methodology to stabilize the monolayer. Therefore, we address the aforementioned question by studying the effect of surface functionalization with H atoms as an effective way to enhance the dynamical stability in monolayer w-gallenene.

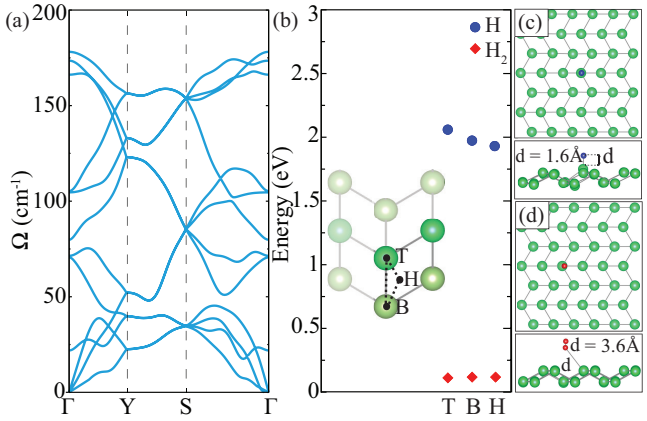

Figure 2: (Color online) (a) Phonon dispersion of 2% uniformly strained *w*-gallenene. (b) The binding energies of the single H adatom and H_2 admolecule on 2% uniformly strained *w*-gallenene surface. The inset shows the possible hydrogenation pathways on the *w*-gallenene surface. The upper Ga atoms are denoted by dark green while the lower ones are denoted by light green. Top and side views of the energetically most favorable adsorption sites of a (c) H atom and (d) single H_2 molecule on $3 \times 3 \times 1$ super cell *w*-gallenene.

1. *Interaction of single H atom and H_2 Molecule with w-gallenene*

Understanding the adsorption properties of a single H atom and H_2 molecule on *w*-gallenene is important in order to understand its hydrogenated derivatives. As seen in Figure 2(b), *w*-gallenene is dynamically stable under 2% biaxial strain. Therefore, the adsorption of a single H atom and H_2 molecule on 2% biaxial strained *w*-gallenene are simulated by considering three inequivalent initial adsorption sites: top of lower Ga atom (B), top of upper Ga atom (T), and hollow (H) site which allows more freedom for taking a position between T and H, as shown in the inset of Figure 2(a).

In order to eliminate H-H and H_2-H_2 interactions, the size of the supercell is chosen to be $3 \times 3 \times 1$. In the case of the H adatom, the bond length of Ga-H is ∼1.61 Å which is close to the electron-diffraction measurement result (∼1.52 Å) of Ga_2H_6.[48] However, in the case of the H_2 admolecule, the distance between Ga and the molecule is calculated to be ∼3.55 Å. The highest binding energy of H adatom is found to be ∼2.21 eV when it is adsorbed on the lower Ga atom. Nevertheless, the highest binding energy of H_2 admolecule is found to be ∼0.29 eV for the case in which H_2 resides on the upper Ga atom. The presence of the *w*-gallenene surface lowers the H_2 molecule adsorption barrier and allows for the

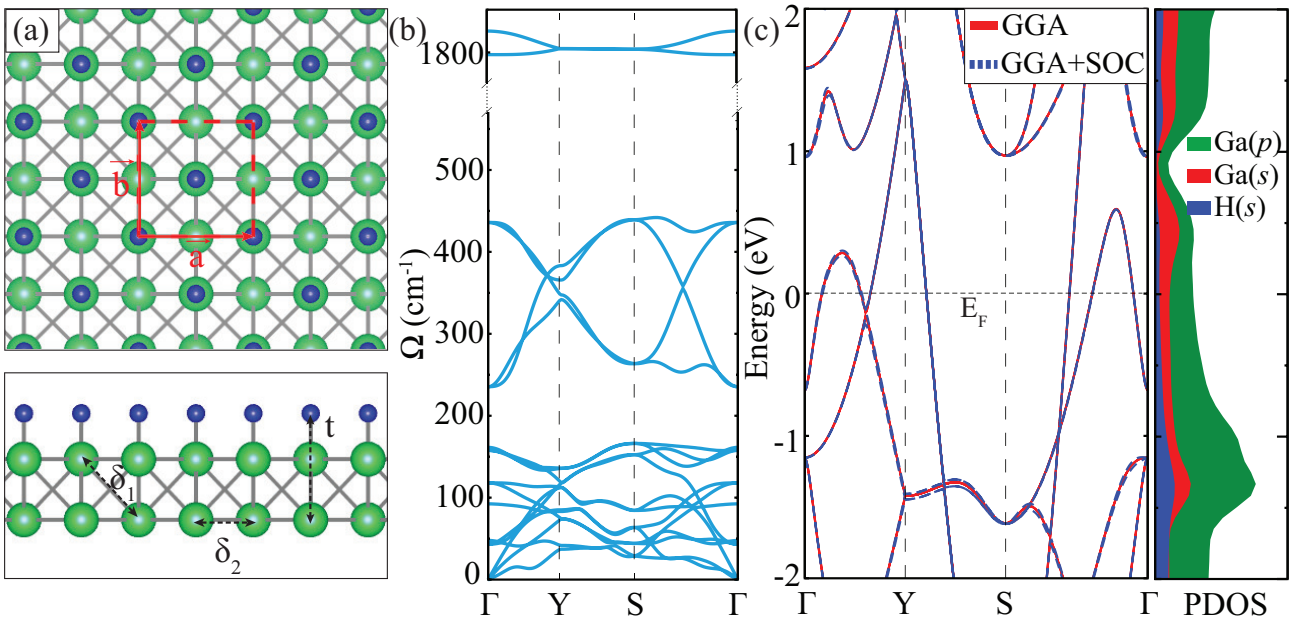

Figure 3: (Color online) (a) Top and side views of os-w-gallenene. Ga and H atoms are denoted by green and blue colors, respectively. Red dashed lines represent the rectangular unit cell; $\vec{a}$ and $\vec{b}$ are the lattice vectors. (b) The phonon band structure of os-w-gallenene. (c) The electronic band structure and corresponding orbital projected partial density of states of os-w-gallenene. The Fermi level is set to zero.

adsorption reaction at energies well below the dissociation threshold of the H-H bond. The H_2 molecule should contain considerable binding energy to be chemically adsorbed by the w-gallenene surface. However, the binding energy is quite low and thus, H_2 is physisorbed on the w-gallenene surface.

As shown in Figs. 2(c) and (d), the local atomic structure is negligibly reconstructed by the adsorbed H atom and H_2 molecule. Based on Bader charge analysis, it is found that Ga atom donates 0.3 e^- to the bonding H atom which reveals the partially ionic bonding between Ga and H atoms. However, due to physisorption of H_2 molecule on w-gallenene, there is no net charge transfer between the surface and the molecule. Moreover, the non-magnetic nature of the monolayer remains unchanged with a single H atom and H_2 molecule adsorptions. Taking into account the analyses of binding energies, bond length, and charge transfer results, hydrogenation of w-gallenene is only possible by using atomic hydrogen.

2. *One-sided Hydrogenation of w-gallenene*

Following the analysis of the adsorption of a single H atom on 2% biaxially strained w-gallenene, in this section, the structural, electronic, and phononic properties of one-sided hydrogenated w-gallenene are discussed. To construct the one-side hydrogenated structure, the most favorable position of an isolated H atom on 2% biaxially strained w-gallenene is considered. After hydrogenation, the applied strain is removed and the system is found to be dynamically stable without biaxial strain. The crystal structure of os-w-gallenene does not retain the structure of w-gallenene as shown in Figure 3(a). The primitive unit cell of os-w-gallenene includes four Ga and two H atoms. The thickness of the monolayer is calculated to be 3.70 Å. The lattice constants are a=b=4.65 Å. The Ga-Ga bond lengths are found to be 2.82 and 2.90 Å for δ_1 and δ_2, respectively.

According to Bader charge analysis, Ga atom donates 0.2 e^- to H atom, i.e., Ga-H bond possesses a partially ionic character while the covalent bonding character between Ga atoms is still conserved. The monolayer os-w-gallenene exhibits a non-magnetic ground state with a cohesive energy of 2.25 eV/atom which is slightly ($\sim$0.07 eV) lower than that of w-gallenene. When H atoms are adsorbed on the w-gallenene surface, strong Ga-H bonds are formed. The work function at the hydrogenated side is increased to $\sim$5.17 eV.

The phonon band structure of monolayer os-w-gallenene is shown in Figure 3(b). After one-sided hydrogenation, the applied strain is removed and the relaxed system is dynamically stable without biaxial strain. Notice that the Ga-H interaction enhances the dynamical stability of monolayer w-gallenene. Monolayer os-w-gallenene exhibits 3 acoustic and 15 optical phonon branches. There are 3 doubly degenerate optical phonon modes having frequencies 43.1, 118.0 and 157.7 cm^{-1} at the Γ point which correspond to in-plane vibration of the atoms. The phonon mode having the frequency 43.1 cm^{-1} is attributed to the opposite in-plane vibration of lower Ga with respect to the upper Ga atoms while the phonon mode with the frequency 118.0 and 157.7 cm^{-1} are attributed to the opposite in-plane vibration of the Ga atoms in each sublayer. In addition, there are 3 optical phonon modes having frequencies of 47.8, 92.4 and 161.4 cm^{-1} at the Γ point, which correspond to out-of-plane vibration of the atoms. The phonon modes with frequency 92.4 and 161.4 cm^{-1} are attributed to out-of-plane vibration of one sublayer Ga while the other sublayer Ga atoms are frozen. However, the phonon mode with frequency 47.8 cm^{-1} is an out-of-plane vibration of lower

Ga with respect to the upper Ga atoms. Furthermore, owing to the smaller atomic radius of the H atom and the relatively strong chemical bonding in os-w-gallenene, the phonon frequencies harden. The modes with higher frequencies occur between 1800-1850 cm^{-1} (see Figure 3(b)), which have only out-of-plane character.

As shown in Figure 3(c), the monolayer os-w-gallenene possesses the characteristic properties of metal with nonzero density of states at the Fermi level. Calculated PDOS reveals that both CB and VB states are mainly made up of the p- and the s-orbitals of Ga atom and s-orbital of H atom. The electronic band structure of os-w-gallenene is highly dispersive with a large bandwidth in the vicinity of the Fermi level, and therefore it possesses high charge carrier mobility. The breaking of spin degeneracy at the CB and VB edges of os-w-gallenene stems from the edge asymmetry of its structure, in strict contrast to w-gallenene.

3. Two-sided Hydrogenation of w-gallenene

In this section, the structural, electronic, and phononic properties of ts-w-gallenene are discussed in detail. In the case of the unstrained ground state, it is found that the crystal structure of ts-w-gallenene is almost the same with that of w-gallenene as shown in Figure 4(a). The primitive unit cell is marked by the red dashed rectangle which contains four Ga and four H atoms. Each Ga atom is saturated with a H atom at the top site. Similar to the case of w-gallenene, it has a buckled structure with a buckling height of 4.44 Å between uppermost and lowermost H atoms. The ts-w-gallenene has a zigzag orthorhombic structure with lattice constants $a = 4.62$ Å and $b = 4.55$ Å. The Ga-Ga bond lengths are found to be 2.72 Å and 2.66 Å for δ_1 and δ_2, respectively.

The Bader charge analysis reveals that each Ga atom donates 0.3 e^- to each H atom, which indicates that the Ga-H bond possesses a partially ionic character. It is seen that the hydrogenation leads to increasing of ionic character of the bonds between Ga and H atoms while the covalency of Ga-Ga bond is still conserved since there occurs no charge transfer between Ga atoms. Similar to the cases of w-gallenene and os-w-gallenene, the ground state structure of the ts-w-gallenene is also found to be non-magnetic. It is found that the cohesive energy for ts-w-gallenene is the same as that of os-w-gallenene. The resulting two-sided hydrogenation of w-gallenene leads to the formation of strong Ga-H bonds. Hence, the ts-w-gallenene has a work function that is $\sim$1.2 eV higher than the one of w-gallenene.

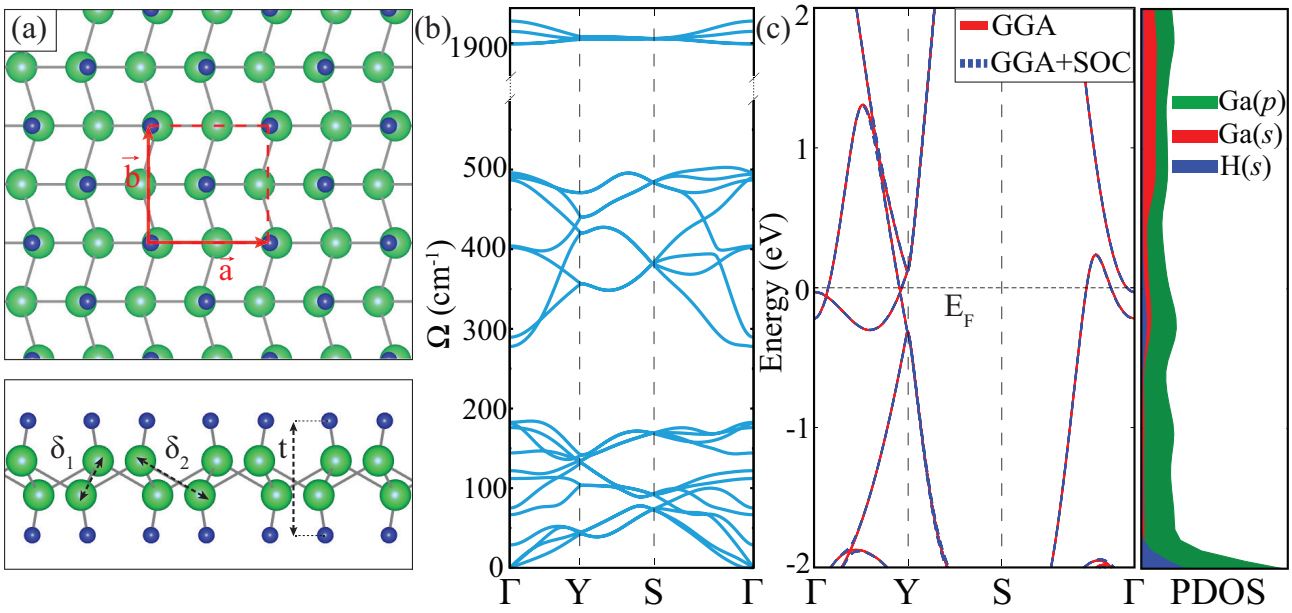

Figure 4: (Color online) (a) Top and side views of ts-w-gallenene. Ga and H atoms are denoted by green and blue colors, respectively. Red dashed lines represent the rectangular unit cell; $\vec{a}$ and $\vec{b}$ are the lattice vectors. (b) The phonon band structure of ts-w-gallenene. (c) The electronic band structure and corresponding orbital projected partial density of states of ts-w-gallenene. The Fermi level is set to zero.

The phonon dispersion of ts-w-gallenene is shown in Figure 4(b). Similar to the case of os-w-gallenene, two-sided hydrogenation of w-gallenene suppress its dynamical instability when the biaxial strain is removed. It exhibits 3 acoustic and 21 optical phonon branches. 2 acoustical phonon branches of the ts-w-gallenene are linear as $k \rightarrow 0$, but its transverse branch displays a quadratic dispersion near the Γ point.

Among the optical vibrational modes, the phonon modes having frequencies 28.8, 66.7, 176.0 and 182.6 cm^{-1} are attributed to the opposite in-plane vibration of Ga with respect to the closest Ga atom. The phonon modes with the frequencies 75.1 and 144.2 cm^{-1} are due to the opposite in-plane vibration of the lower Ga with respect to the upper Ga atoms. The phonon modes at frequencies 112.1 and 121.9 cm^{-1} are attributed to the opposite out-of-plane vibration of Ga with respect to the closest Ga atom. Furthermore, the phonon mode having frequency 180.9 cm^{-1} reveals the opposite out-of-plane vibration of the lower Ga with respect to the upper Ga atoms. Similar to the case of os-w-gallenene, Ga-H bonds have much higher frequencies than the Ga-Ga bonds as shown in Figure 4(b). The higher

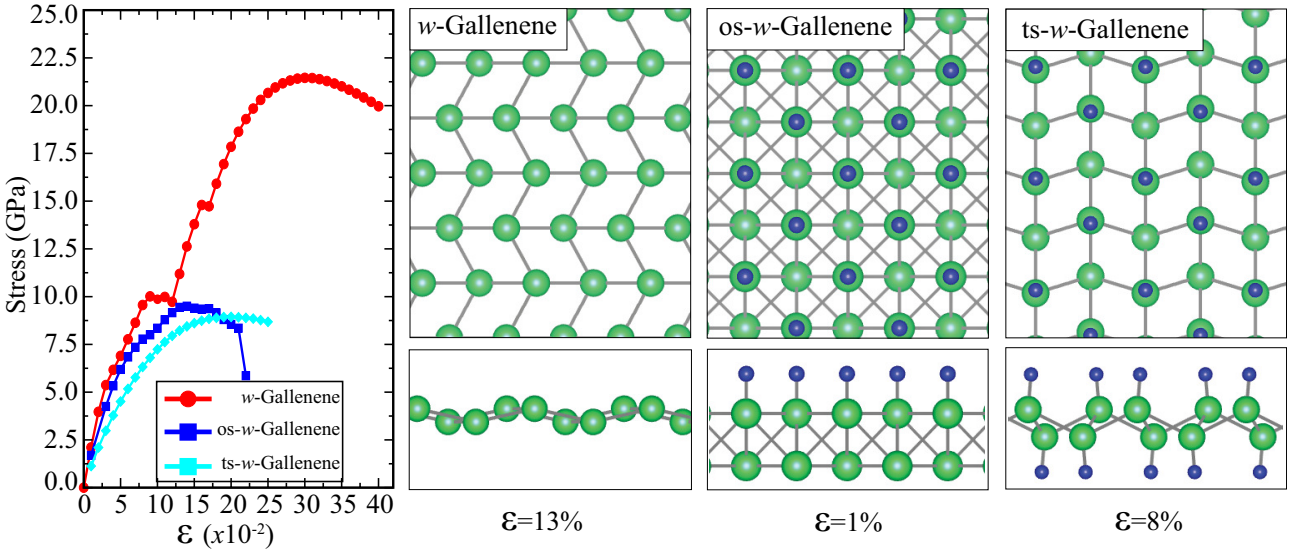

Figure 5: (Color online) The left panel shows the stress-strain energy curves under applied biaxial strain for 3 monolayers. Right panel, the crystal structures of the three different monolayers are shown at the maximum biaxial strains after which the phononic instabilities occur.

frequencies out-of-plane modes between 1940-2000 cm^{-1} indicate the formation of strong Ga-H bonds as well.

As shown in Figure 4(c), the ts-*w*-gallenene also possesses metallic character because of the finite density of states at the Fermi energy. It is found from the PDOS calculation that the CB states are mainly made up of the *p*- and *s*-orbitals of the Ga atoms, whereas the states in the VB have the character of *p*-orbital of Ga atom and *s*-orbital of H atom. Unlike os-*w*-gallenene, there is a notable change in the dispersion in the vicinity of the Fermi level. The bands of *w*-gallenene only cross at the Fermi level between the Y and Γ high symmetry points. As in the case of *w*-gallenene, negligibly small spin-orbit splittings occur in the low energy valence bands. Furthermore, similar to the cases of *w*-gallenene and os-*w*-gallenene, the electronic bands of *w*-gallenene are highly dispersive with a large bandwidth in the vicinity of the Fermi level which indicates a high charge carrier mobility.

C. Mechanical Properties of *w*-gallenene, os- and ts-*w*-gallenene

The mechanical properties of the monolayers, *w*-gallenene, os- and ts-*w*-gallenene, are discussed in terms of their linear-elastic parameters. The linear-elastic properties of two-

dimensional homogeneous monolayer materials can be represented by two independent constants, the in-plane stiffness, C, and the Poisson ratio, ν.

The linear-elastic constants of the monolayer w-gallenene, os- and ts-w-gallenene are determined by using the energy-strain relation. 64-, 96- and 128-atom super cells are constructed for bare, os- and ts-w-gallenene crystals, respectively. The tensile and compressive strains are applied along the a and b vectors, respectively. The strain parameters ε_a and ε_b are varied between ± 0.015 with a step size of 0.005. Then, three different sets of data are calculated; (i) ε_a=0 and ε_b varying, (ii) ε_b=0 and ε_a varying and (iii) ε_a=ε_b varying. At each configuration, the atomic positions are fully relaxed and the strain energy, E_S, is calculated by subtracting the total energy of the equilibrium state from the strained structure. Then, the calculated data is fitted to the equation; $E_S = c_1{\varepsilon_a}^2 + c_2{\varepsilon_b}^2 + c_3\varepsilon_a\varepsilon_b$[49], and the coefficients c_i are determined.

The in-plane stiffness, C, is a measure of the rigidity of a material under applied load. For a 2D crystal, the larger C demonstrates less stretchability of the material. In isotropic monolayers, no orientational dependence in the crystal is expected. However, if there is even a small anisotropy in the material the stiffness along the two lattice vectors is given by; $C_a = (1/A_0)(2c_1 - {c_3}^2/2c_2)$[50] and $C_b = (1/A_0)(2c_2 - {c_3}^2/2c_1)$[50] where $c_1 \neq c_2$ due to the anisotropy of the crystal structure and A_0 is the area of the unstrained super cell. The rigidity of monolayer w-gallenene may clearly be understood by comparing its in-plane stiffness with that of other mono-atomic 2D materials. We find $C_a \approx C_b \approx 25$ N/m (see Table 1) which is practically isotropic. When compared with that of graphene (330 N/m[51]) monolayer w-gallenene has a very small in-plane stiffness which is a consequence of the relatively weak Ga-Ga bonds in the crystal. For mono-atomic crystals of Si and Ge, respectively, stiffnesses 62 and 48 N/m were reported[51] which are even higher than that of w-gallenene. Very low in-plane stiffness of w-gallenene reveals that it withstands high values of strain at low stresses.

In the case of os-w-gallenene, the presence of H atoms results in an increase in the stiffness and the calculated stiffnesses are $C_a \approx C_b \approx 52$ N/m indicating the isotropic nature of the crystal structure. Increased in-plane stiffness expresses itself in the higher phonon frequencies as shown in Figure 3(b). The same trend is found for the monolayer ts-w-gallenene whose in-plane stiffnesses, C_a=48 N/m and C_b=47 N/m, are slightly different along the two directions. In contrast to other hydrogenated monolayer crystals, graphane[52–54] and 1T-ReS_2H_2[31], which

softens when hydrogenated, in the case of w-gallenene surface-hydrogenation forms relatively strong Ga-H bonds which tunes the Ga-Ga bonds resulting in an increased in-plane stiffness.

The Poisson ratio of a material is defined as the ratio of the transverse contraction strain to the longitudinal extension strain in the direction of the stretching force, that is $\nu{=}\varepsilon_{trans}/\varepsilon_{long}$. The Poisson ratio for a- and b-vectors can be calculated in terms of the coefficients c_i as; $\nu_a{=}c_3/2c_2$ and $=c_3/2c_1$. The Poisson ratios for w-gallenene are $\nu_a \approx \nu_b \approx 0.20$. These values are smaller as compared to those for the well-known TMDs, i.e., 0.25 for MoS_2[55], 0.22 for WS_2[55], and 0.23 for $MoSe_2$[55]. The Poisson ratio displays different behavior depending on the type of hydrogenation in the case of w-gallenene. For the monolayer os-w-gallenene it is 0.26 which is larger than that of graphene (0.19)[51]. This indicates a larger extension of the crystal in the transverse direction when it is contracted along the longitudinal direction. However, when both surfaces are hydrogenated the Poisson ratio are $\nu_a \approx \nu_b \approx 0.25$.

The ultimate strength of a material is the maximum value of stress that a material can resist before fracturing. This value can be directly investigated from the maximum point of the stress-strain curve of a material. In order to investigate the non-linear-elastic properties of the Gallium monolayers, the large biaxial strain is applied to the crystals. As seen on the left panel of Figure 5, monolayers of w-gallenene and its derivatives do not exhibit a fracture even at large biaxial strain. The ultimate strength of monolayer w-gallenene is calculated to be 22 GPa which is much lower than that of graphene (96 GPa[28]), but close to that of monolayer MoS_2 (26 GPa[28]) and even much higher than those of Ga-monochalcogenides (12 and 10 GPa for GaS and GaSe, respectively)[28]. In addition, the ultimate strain value, that is the strain at which the material exhibits its ultimate strength, is higher (30% for monolayer w-gallenene) than those for Ga-monochalcogenides (24% and 23% for GaS and GaSe, respectively)[28]. Furthermore, we analyze the phonon instability under applied biaxial strain. As shown on the right panel of Figure 5, the maximum biaxial strains are 13, 1 and 8% for w-gallenene, os-w-gallenene and ts-w-gallenene, respectively; for which the phonon instabilities occur. Especially, the phonon stabilities of w-gallenene against biaxial tensile strain values are higher than for the super-stretchable borophene (8%).[56]

In contrast to the results for the linear-elastic parameters, hydrogenation of w-gallenene decreases both the ultimate strength and strain values. In the case of one-sided hydrogenation, the material withstands a maximum load of 12 GPa at a relatively much lower strain

value of 14%. After monolayer os-w-gallenene exhibits its maximum stress at 14% of biaxial strain, it does not show a crystal fracture up to a strain value of 22% at which there is a sharp decrease in the stress (see Figure 5). However, the phonon instability occurs just at 1% of biaxial strain which suggests that one-sided hydrogenation is probably not feasible. In the case of monolayer ts-w-gallenene, the ultimate strength shows a decrease in stress to 9 GPa, but at a larger strain value of 20%. This larger ultimate strain can be related to the distorted Ga-H bonds at both surfaces which are more flexible than those in monolayer os-w-gallenene. As seen in Figure 5, the phonon instability occurs at 8% of the biaxial strain which is the same as that of borophene itself (8%).[56]

In order to characterize the corrugation of 2D materials, the buckling height, t, is an important parameter.[57,58] The buckling height decreases monotonously with increasing strain before the strain approaches the critical value (12%), but it quickly decreases to zero as the strain continuously increases. Until applying 8% biaxial tensile strain, w-gallenene possesses more superior flexibility and isotropic character because it perceives approximately the same in-plane a and b directional stress. However, there is different a and b directional tension between applying 8% and 12% tensile strain, so the stress-dependent buckling height is non-monotonic. Between the stresses 12% to 17%, the structure is elongated differently in the x and y directions which increases its anisotropy. Hence, w-gallenene turns into a graphene-like planar structure instead of the original bucking structure in this case.

IV. CONCLUSIONS

The structural, phononic, electronic and mechanical properties of pristine and hydrogenated monolayers of w-gallenene were investigated within state-of-the-art first-principles calculations. We showed that a single H atom can be adsorbed to the surface of w-gallenene with high binding energy (2.21eV). One- and two-sided hydrogenated w-gallenene are dynamically stability. Electronic structure calculations revealed that all monolayers, w-gallenene, os-w-gallenene and ts-w-gallenene, are non-magnetic, metals. Moreover, the linear-elastic constants, in-plane stiffness and Poisson ratio, of monolayer w-gallenene are enhanced by one- and two-sided hydrogenation which is the opposite trend found for other hydrogenated monolayer crystals. However, in the non-linear-elastic regime, it was found that the ultimate strength and the ultimate strain decrease as the number of

hydrogenated surfaces increase. Moreover, the phonon stabilities of monolayer w-gallenene and ts-w-gallenene remain up to relatively higher biaxial strains when compared to borophene. With its enhanced dynamical stability, robust metallic character, and enhanced linear-elastic properties, hydrogenated monolayer w-gallenene is a potential candidate for nanodevice applications as a 2D flexible metal.

Supporting Information Available: The electonic band structures of w -gallenene, os- and ts-w -gallenene by using GGA, LDA, GGA+HSE and META-GGA functionals are reported in Figure S1. The thermal stability of the all monolayer Gallenene crystals are presented in Figure S2.

Acknowledgments

Computational resources were provided by TUBITAK ULAKBIM, High Performance and Grid Computing Center (TR-Grid e-Infrastructure). H.S. acknowledges financial support from the Scientific and Technological Research Council of Turkey (TUBITAK) under the project number 117F095. This work was supported by FLAG-ERA project TRANS-2D-TMD. This work is supported by the Flemish Science Foundation (FWO-Vl) by a post-doctoral fellowship (M.Y.).

* Electronic address: sabuhibadalov@iyte.edu.tr

† Electronic address: mehmetyagmurcukardes.edu@gmail.com

References

[1] Novoselov, K. S.; Geim, A. K.; Morozov, S. V.; Jiang, D.; Zhang, Y.; Dubonos, S. V.; Grigorieva, I. V.; Firsov, A. A. Electric Field Effect in Atomically Thin Carbon Films. *Science.* **2004**, 306, 666-669.

[2] Geim, A. K.; Novoselov, K. S. The Rise of Graphene. *Nat. Mater.* **2007**, 6, 183-191.

[3] Kim, K. K.; Hsu, A.; Jia, X.; Kim, S. M.; Shi, Y.; Hofmann, M.; Nezich, D.; Rodriguez-Nieva, J. F.; Dresselhaus, M.; Palacios, T.; Kong, J. Synthesis of Monolayer Hexagonal Boron Nitride

on Cu Foil Using Chemical Vapor Deposition. *Nano Lett.* **2012**, 12, 161-166.

[4] Manzeli, S.; Ovchinnikov, D.; Pasquier, D.; Yazyev, O. V.; Kis, A. 2D transition metal dichalcogenides. *Nat. Rev. Mater.* **2017**, 2, 17033.

[5] Coleman, J. N.; Lotya, M.; O'Neill, A.; Bergin, S. D.; King, P. J.; Khan, U.; Young, K.; Gaucher, A.; De, S.; Smith, R. J.; et al. Two-dimensional nanosheets produced by liquid exfoliation of layered materials. *Science.* **2011**, 331, 568-571.

[6] Chhowalla, M.; Shin, H. S.; Eda, G.; Li, L. J.; Loh, K. P.; Zhang, H. The chemistry of two-dimensional layered transition metal dichalcogenide nanosheets. *Nat. Chem.* **2013**, 5, 263-275.

[7] Kara, A.; Enriquez, H.; Seitsonen, A. P.; Voon, L. C. L. Y.; Vizzini, S.; Aufray, B.; Oughaddou, H.; A review on silicenenew candidate for electronics. *Surf. Science Report.* **2012**, 67, 1-18.

[8] Vogt, P.; Padova, P.; Quaresima, C.; Avila, J.; Frantzeskakis, E.; Asensio, M. C.; Resta, A.; Ealet, B.; Lay, G. L. Silicene: Compelling Experimental Evidence for Graphenelike Two-Dimensional Silicon. *Phys. Rev. Lett.* **2012**, 108, 155501.

[9] Padova, P. D.; Kubo, O.; Olivieri, B.; Quaresima, C.; Nakayama, T.; Aono, M.; Lay, G. L. Multilayer Silicene Nanoribbons. *Nano Lett.* **2012**, 12, 5500-5503.

[10] Bianco, E.; Butler, S.; Jiang, S.; Restrepo, O. D.; Windl, W.; Goldberger, J. E. Stability and exfoliation of germanane: a germanium graphane analogue. *ACS Nano.* **2013**, 7, 4414-4421.

[11] Derivaz, M.; Dentel, D.; Stephan, R.; Hanf, M. C.; Mehdaoui, A.; Sonnet, P.; Pirri, C. Continuous Germanene Layer on Al(111). *Nano Lett.* **2015**, 15, 2510-2516.

[12] Dávila, M. E.; Xian, L.; Cahangirov, S.; Rubio, A.; Lay, G. L. Germanene: a novel two-dimensional germanium allotrope akin to graphene and silicene. *New J. Phys.* **2014**, 16, 095002.

[13] Dávila, M. E.; Lay, G. L. Few layer epitaxial germanene: a novel two-dimensional Dirac material. *Sci. Rep.* **2016**, 6, 20714.

[14] Zhu, F.-f.; Chen, W.-j.; Xu, Y.; Gao, C.-l.; Guan, D.-d.; Liu, C.-h.; Qian, D.; Zhang, S.-C.; Jia, J.-f. Epitaxial Growth of Two-Dimensional Stanene. *Nat. Mater.* **2015**, 14, 1020-1025.

[15] Saxena, S.; Chaudhary, R. P.; Shukla, S. Stanene: Atomically Thick Free-standing Layer of 2D Hexagonal Tin. *Sci. Rep.* **2016**, 6, 31073.

[16] Li, L.; Yu, Y.; Ye, G. J.; Ge, Q.; Ou, X.; Wu, H.; Feng, D.; Chen, X. H.; Zhang, Y.; Black phosphorus field-effect transistors. *Nat. Nanotechnol.* **2014**, 9, 372-377.

[17] Sachdev, H.; Disclosing boron's thinnest side. *Science.* **2015**, 350, 1468-1469.

[18] Bernasconi, M.; Chiarotti, G. L.; Tosatti, E. *Ab initio* calculations of structural and electronic

properties of gallium solid-state phases. *Phys. Rev. B.* **1995**, 52, 9988-9998.

[19] Kenichi, T.; Kazuaki, K.; Masao, A. High-pressure bct-fcc phase transition in Ga. *Phys. Rev. B.* **1998**, 58, 2482-2486.

[20] Bosio, L. Crystal structures of Ga(II) and Ga(III). *J. Chem. Phys.* **1978**, 68, 1221-1223.

[21] Steenbergen. K. G.; Gaston, N. First-principles melting of gallium clusters down to nine atoms: structural and electronic contributions to melting. *Phys. Chem. Chem. Phys.* **2013**, 15, 15325-15332.

[22] Schulte, O.; Holzapfel, W. Effect of pressure on the atomic volume of Ga and Tl up to 68 GPa. *Phys. Rev. B.* **1997**, 55, 8122-8128.

[23] Hall, R. N.; Fenner, G. E.; Kingsley, J. D.; Soltys, T. J.; Carlson, R. O. Coherent Light Emission From GaAs Junctions. *Phys. Rev. Lett.* **1962**, 9, 366-369.

[24] Amano, H.; Sawaki, N.; Akasaki, I,; Toyoda, Y. Metalorganic vapor phase epitaxial growth of a high quality GaN film using an AlN buffer layer. *App. Phys. Lett.* **1986**, 48, 353-355.

[25] Zhang, H.-M.; Sun, Y.; Li, W; Peng, J.-P.; Song, C.-L.; Xing, Y.; Zhang, Q.; Guan, J.; Li, Z.; Zhao, Y.; et al. Detection of a Superconducting Phase in a Two-Atom Layer of Hexagonal Ga Film Grown on Semiconducting GaN(0001). *Phys. Rev. Lett.* **2015**, 114, 107003.

[26] Zhou, X.; Cheng, J.; Zhou, Y.; Cao, T.; Hong, H.; Liao, Z.; Wu, S.; Peng, H.; Liu, K.; Yu, D. Strong Second-Harmonic Generation in Atomic Layered GaSe. *J. Am. Chem. Soc.* **2015**, 137, 7994-7997.

[27] Carey, B. J.; Ou, J. Z.; Clark, R. M.; Berean, K. J.; Zavabeti, A.; Chesman, A. S. R.; Russo, S. P.; Lau, D. W. M.; Xu, Z.-Q.; Bao, Q.; et al. Wafer-scale two-dimensional semiconductors from printed oxide skin of liquid metals. *Nat. Commun.* **2017**, 8, 14482.

[28] Yagmurcukardes, M.; Senger, R. T.; Peeters, F. M.; Sahin, H.; Mechanical properties of monolayer GaS and GaSe crystals. *Phys. Rev. B.* **2016**, 94, 245407.

[29] Xing, Y.; Zhang, H.-M.; Fu, H.-L.; Liu, H.; Sun, Y.; Peng, J.-P.; Wang, F.; Lin, X.; Ma, X.-C.; Xue, Q.-K.; et al. Quantum Griffiths singularity of superconductor-metal transition in Ga thin films. *Science.* **2015**, 350, 542-545.

[30] Kochat, V.; Samanta, A.; Zhang, Y.; Bhowmick, S.; Manimunda, P.; Asif, S.; Stender, A. S.; Vajtai, R.; Singh, A. K.; et al. Atomically thin gallium layers from solid-melt exfoliation. *Sci. Adv.* **2018**, 4, e1701373.

[31] Yagmurcukardes, M.; Bacaksiz, C.; Senger, R. T.; Sahin, H. Hydrogen-induced structural tran-

sition in single layer ReS_2. *2D Materials.* **2017** 4, 035013.

[32] Li, W.; Kong, L.; Feng, B.; Fu, H.; Li, H.; Zeng, X. C.; Wu, K.; Chen, L. Abnormal phase transition between two-dimensional high-density liquid crystal and low-density crystalline solid phases. *Nat. Com.* **2018**, 9, 198.

[33] Lei, B.; Pan, Y.; Hu, Z.; Zhang, J.; Xiang, D.; Zheng, Y.; Guo, R.; Han, C.; Wang, L.; Lu, J.; et al. Direct Observation of Semiconductor-Metal Phase Transition in Bilayer Tungsten Diselenide Induced by Potassium Surface Functionalization. *ACS Nano.* **2018**, 12, 2070-2077.

[34] Ma, Y.; Liu, B.; Zhang, A.; Chen, L.; Fathi, M.; Shen, C.; Abbas, A. N.; Ge, M.; Mecklenburg, M.; Zhou, C. Reversible Semiconducting-to-Metallic Phase Transition in Chemical Vapor Deposition Grown Monolayer WSe_2 and Applications for Devices. *ACS Nano.* **2015**, 9, 7383-7391.

[35] Radhakrishnan, S.; Das, D.; Samanta, A.; Reyes, C. A. d. l.; Deng, L.; Alemany, L. B.; Weldeghiorghis, T. K.; Khabashesku, V. N.; Kochat, V.; Jin, Z.; et al. Fluorinated h-BN as a magnetic semiconductor. *Sci. Adv.* **2017**, 3, e1700842.

[36] Hever, A.; Bernstein, J.; Hod, O. Fluorination Effects on the Structural Stability and Electronic Properties of sp^3-type Silicon Nanotubes. *J. Phys. Chem. C.* **2013**, 117, 14684-14691.

[37] Perdew, J. P.; Burke, K.; Ernzerhof, M. Generalized Gradient Approximation Made Simple. *Phys. Rev. Lett.* **1996**, 77, 3865-3868.

[38] Kresse, G.; Furthmuller, J. Efficient iterative schemes for *ab initio* total-energy calculations using a plane-wave basis set. *Phys. Rev. B.* **1996**, 54, 11169-11186.

[39] Henkelman, G.; Arnaldsson, A.; Jonsson, H. A fast and robust algorithm for Bader decomposition of charge density. *Comput. Mater. Sci.* **2006**, 36, 354-360.

[40] Alfe, D.; PHON: A program to calculate phonons using the small displacement method. *Comp. Phys. Commun.* **2009**, 180, 2622-2633.

[41] Yu, Y. J.; Zhao, Y.; Ryu, S.; Brus, L. E.; Kim, K. S.; Kim, P. Tuning the Graphene Work Function by Electric Field Effect. *Nano Lett.* **2009**, 9, 3430-3434.

[42] Chen, M. X.; Zhong, Z.; Weinert, M.; Designing substrates for silicene and germanene: First-principles calculations. *Phys. Rev. B.* **2016**, 94, 075409.

[43] Zhou, S.; Zhao, J. Electronic Structures of Germanene on MoS_2: Effect of Substrate and Molecular Adsorption. *J. Phys. Chem. C.* **2016**, 120, 21691-21698.

[44] Garg, P.; Choudhuri, I.; Mahata, A.; Pathak, B. Band gap opening in stanene induced by patterned BN doping. *Phys. Chem. Chem. Phys.* **2017**, 19, 3660-3669.

[45] Liu, F.; Ming, P.; Li, J. *ab initio* calculation of ideal strength and phonon instability of graphene under tension. *Phys. Rev. B.* **2007**, 76, 064120.

[46] Cahangirov, S.; Topsakal, M.; Aktürk, E.; Sahin, H.; Ciraci, S. Two- and One-Dimensional Honeycomb Structures of Silicon and Germanium. *Phys. Rev. Lett.* **2009**, 102, 236804.

[47] Cassabois, G.; Valvin, P.; Gil, B. Hexagonal boron nitride is an indirect bandgap semiconductor. *Nat. Photonics.* **2016**, 16, 262-266.

[48] Pulham, C. R.; Downs, A. J.; Goode, M. J.; Rankin, D. W. H.; Robertson, H. E. Gallane: synthesis, physical and chemical properties, and structure of the gaseous molecule Ga_2H_6 as determined by electron diffraction. *J. Am. Chem. Soc.* **1991**, 113, 5149-5162.

[49] Nye, J. F. *Physical Properties of Crystals: Their Representation by Tensors and Matrices;* Clarendon Press: Oxford, **1985**.

[50] Kang, J.; Sahin, H.; Peeters, F. M. Mechanical properties of monolayer sulphides: a comparative study between MoS_2, HfS_2 and TiS_3. *Phys. Chem. Chem. Phys.* **2015**, 17, 27742-27749.

[51] Sahin, H.; Cahangirov, S.; Topsakal, M.; Bekaroglu, E.; Aktürk, E.; Senger, R. T.; Ciraci, S. Monolayer honeycomb structures of group-IV elements and III-V binary compounds: First-principles calculations. *Phys. Rev. B.* **2009**, 80, 155453.

[52] Topsakal, M.; Cahangirov, S.; Ciraci, S. The response of mechanical and electronic properties of graphane to the elastic strain. *Appl. Phys. Lett.* **2010**, 96, 091912.

[53] Peelaers, H.; Hernandez-Nieves, A. D.; Leenaerts, O.; Partoens, B.; Peeters, F. M. Vibrational properties of graphene fluoride and graphane. *Appl. Phys. Lett.* **2011**, 98, 051914.

[54] Leenaerts, O.; Peelaers, H.; Hernndez-Nieves, A. D.; Partoens, B.; Peeters, F. M. First-principles investigation of graphene fluoride and graphane. *Phys. Rev. B.* **2010**, 82, 195436.

[55] Guzman. D. M.; Strachan, A. Role of strain on electronic and mechanical response of semiconducting transition-metal dichalcogenide monolayers: An *ab-initio* study. *J. Appl. Phys.* **2014**, 115, 243701.

[56] Wang, H.; Li, Q.; Gao, Y.; Miao, F.; Zhou, X. F.; Wan, X. G. Strain effects on borophene: ideal strength, negative Possions ratio and phonon instability. *New J. Phys.* **2016**, 18, 073016.

[57] Wei, Q.; Peng, X. Superior mechanical flexibility of phosphorene and few-layer black phosphorus. *Appl. Phys. Lett.* **2014**, 104, 251915.

[58] Hu, T.; Han, Y.; Dong, J. M. Mechanical and electronic properties of monolayer and bilayer phosphorene under uniaxial and isotropic strains. *Nanotechnology.* **2014**, 25, 455703.

TOC Graphic

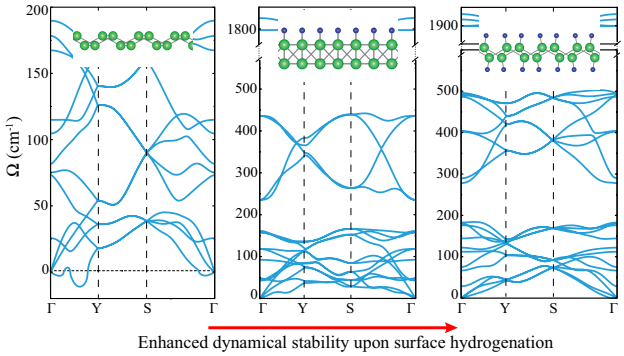
Ω (cm⁻¹)
Γ Y S Γ
Enhanced dynamical stability upon surface hydrogenation